International Journal of Advances in Scientific Research and Engineering (ijasre)

E-ISSN : 2454-8006

DOI: 10.31695/IJASRE.2025.10.1

Volume 11, Issue 10
October- 2025

Biosynthesis of Silver Nanoparticles and Its Effects on the Establishment *in vitro* of Cassava (*Manihot esculenta*)

Ashton Daniels[1], Dion Daniels[1*], Chelsea Herrera[2], Tysha Daniels[3], and Ainsley Ferguson[3]

[1]Science Department, Faculty of Science & Technology, University of Belize

[2]Hummingbird Analytical Laboratory, University of Belize

[3]MPIT Department, Faculty of Science & Technology, University of Belize

Belize

ABSTRACT

Cassava (Manihot esculenta) is a staple crop in Belize, yet efficient in vitro propagation remains challenged by microbial contamination and inconsistent explant development. Silver nanoparticles (AgNPs) offer antimicrobial and growth-modulating benefits. This study compared green-synthesized versus commercial AgNPs on the establishment in vitro of cassava var. "white". Green AgNPs were biosynthesized using Moringa oleifera extract with $AgNO_3$ and characterized by UV–Vis and FTIR; commercial AgNPs (XFNANO) served as a reference. Nodal explants were cultured on Murashige and Skoog medium with 1 mg/L 6-benzylaminopurine, 1 mg/L α-naphthaleneacetic acid, and AgNPs at 0, 5, 10, and 15 mg/L. After five weeks, shoot and root lengths were recorded. Contamination percentages were also evaluated. Data were analyzed by one-way ANOVA with Tukey's HSD for parametric cases and Kruskal–Wallis with Dunn's post-hoc when assumptions failed. Commercial silver nanoparticles significantly enhanced shoot elongation in a dose-dependent manner, with the 15 mg/L treatment producing a mean shoot length of 1.82 ± 3.27 cm compared to 0.12 ± 0.41 cm in the control group ($p < .001$). Root growth was also stimulated, reaching 0.44 ± 0.90 cm versus 0 cm in controls ($p = 0.0003$). In contrast, green-synthesized AgNPs inhibited shoot elongation at 5 mg/L, reducing mean shoot length to 0.38 ± 1.19 cm from 2.20 ± 3.70 cm ($p < .001$), while root length fell to 0.07 ± 0.26 cm compared to 0.76 ± 1.57 cm in untreated plants ($p = 0.0002$). Nonparametric tests confirmed these trends under non-normal data distributions. The variance ranged from medium to large, indicating robust treatment effects. Commercial AgNPs can promote initial explant growth, while plant-extract–derived AgNPs at tested doses exert phytotoxicity. These contrasting outcomes underscore that nanoparticle source and concentration must be optimized to balance antimicrobial control with plant growth.

Keywords: Green Synthesis, *Manihot esculenta*, Micropropagation, Silver Nanoparticles.

1. INTRODUCTION

The application of nanoparticles in plant tissue culture has emerged as a dynamic field of research that seeks to improve the efficiency and outcomes of *in vitro* cultivation. Among the various nanoparticles explored, silver nanoparticles (AgNPs) have attracted significant interest due to their potent antimicrobial properties and their ability to modulate plant growth responses. In plant tissue culture, contamination control is paramount, and AgNPs offer a promising alternative to conventional chemical sterilant. Silver nanoparticles are typically synthesized through chemical reduction, green synthesis using plant extracts, or biological methods that employ microbial agents. Their small size and large surface area facilitate interactions with cellular components, which is critical for both their antimicrobial action and their influence on plant physiology. In tissue culture, AgNPs have been reported to suppress bacterial and fungal contaminants by disrupting cell membranes and generating reactive oxygen species (ROS). AgNPs interact with microbial cell membranes, leading to oxidative stress and cell death through ROS production and membrane rupture. Their small size (1.5–26 nm) allows them to diffuse easily into cells (Kalwar & Shan, 2018). The

antimicrobial action helps to maintain sterile conditions in culture media, thereby reducing the need for conventional antibiotics, which can sometimes lead to resistance or phytotoxic effects. Studies consistently show that AgNPs not only reduce contamination but also support better callus induction and explant viability, offering a dual benefit over traditional antibiotics that can cause phytotoxicity or resistance (Alfarraj et al., 2023).

Beyond their antimicrobial benefits, AgNPs have been shown to influence morphogenetic responses in plant tissue cultures. Research indicates that AgNPs can stimulate the formation of callus tissue, promote shoot induction, and even enhance root development in certain plant species. For instance, experiments in cassava tissue cultures have revealed that the incorporation of silver nanoparticles in the culture media not only minimizes contamination, but also improves explant survival and regeneration rates. The underlying mechanisms appear to be related to the modulation of plant hormones such as auxins and cytokinins, which play a pivotal role in cell division and differentiation. AgNPs of different shapes influenced growth responses in Arabidopsis, including root elongation and gene expression tied to auxin, ethylene, and stress signaling. The decahedral form promoted root growth most effectively (Syu et al., 2014). Wheat AgNPs altered hormone levels, leading to accelerated flowering and improved yield in wheat. Effects differed from silver ions, underscoring nanoparticle-specific activity (Pociecha et al., 2021). Current studies provide a compelling case for the broader use of nanotechnology in plant biotechnology, as AgNPs offer the advantage of enhanced microbial control and improved plant tissue responsiveness.

However, the application of silver nanoparticles is not without challenges. Concerns remain regarding the optimal concentration, potential phytotoxicity, and the long-term environmental impact of nanoparticle use. Despite their benefits, AgNPs can alter soil microbial communities and have unintended ecological effects, particularly when overused or improperly managed (Courtois et al., 2019). Detailed dose–response experiments are necessary to establish safe and effective protocols. Long-term exposure to environmentally relevant concentrations of AgNPs has been shown to affect major soil bacterial phyla, highlighting concerns about their prolonged environmental presence (Grün & Emmerling, 2018). Additionally, the interaction between AgNPs and plant tissues at the molecular level is an area of ongoing investigation. Researchers are exploring how nanoparticles might influence gene expression related to stress responses, secondary metabolite production, and defense mechanisms. Proteomic studies have been instrumental in elucidating the complex molecular pathways involved in plant responses to nanoparticle-induced stress (Hossain et al., 2015).

Cassava (*Manihot esculenta*), also known as yuca or manioc, is a crop that holds much importance worldwide, but also in the country of Belize, where it is a staple crop that is renowned for its economic significance. Cassava also fuels the livelihoods of smallholder farmers in tropical regions (Chavez et al., 2021). Cassava is among the top three most widely produced root crops in the world. In 2022, global cassava production reached roughly 330 million tons, nearly double the level in 2000 (FAOSTAT Analytical Briefs, 2023). This extends an upward trend seen in recent decades, with production increasing from approximately 286 million tons in 2017 to 315 million tons in 2021 (Otekunrin, 2024). Africa is the largest producing region, accounting for about 208 million tons (over 60% of world output in 2022). Asia contributes nearly 96 million tons, and the Americas about 26 million. The leading producer is Nigeria, which harvested approximately 60–63 million tons in recent years (around 20% of global production) (FAOSTAT Analytical Briefs, 2023).

Although cassava has a rich historical presence in Belize, its cultivation remains relatively limited in scale. Belize's current production is estimated at 1,316 MT, with a planted area of 107 ha and productivity of 12 MT per ha (Ospina et al., 2016). Cassava plays an essential role in the Garifuna culture in Belize, where it is used to make cassava bread and other foods. The Garifuna language even has more than 10 different words for cassava in its various forms. The crop is primarily grown in the southern districts of Stann Creek and Toledo, where the Garifuna and other communities cultivate it for home use and local markets. These areas have cultivated cassava for generations. For instance, people in the Stann Creek District have traditionally grown cassava as a subsistence crop well-suited to the district's cultural and climatic conditions.

DOI: 10.31695/IJASRE.2025.10.1

This study hypothesizes that incorporating biosynthesized green silver nanoparticles in the culture media for the establishment *in vitro* of cassava (*Manihot esculenta*) will significantly enhance plant growth by promoting longer shoots and reducing microbial contamination compared to cultures with commercial silver nanoparticles and without nanoparticle treatment. To evaluate this, the study will first develop and validate an eco-friendly synthesis protocol for producing silver nanoparticles using plant extracts. Subsequently, the research will assess the effects of these nanoparticles on the establishment *in vitro* of cassava explants by measuring key growth parameters, including shoot length, and root development as well as monitoring contamination levels in the cultures. Finally, a comparative analysis between treated explants and untreated controls will be conducted to ascertain the practical benefits and potential advantages of using green-synthesized nanoparticles in improving the establishment *in vitro* of cassava.

2. MATERIALS AND METHODS

This study was conducted at the Micropropagation Laboratory and the Hummingbird Analytical Laboratory in the Faculty of Science & Technology, University of Belize, Belmopan, Belize.

2.1 BIOSYNTHESIS OF SILVER NANOPARTICLES (AgNPs)

The biosynthesis of green silver nanoparticles (AgNPs) was carried out at the Hummingbird Analytical Laboratory at the University of Belize. It was achieved using a plant extract-based approach. A 0.33M solution of silver nitrate ($AgNO_3$) was prepared by weighing out 16.987 grams of silver nitrate and dissolved in three hundred (300) mL of distilled water in an Erlenmeyer flask. To create a solution of moringa (*Moringa oleifera*) extract, ten (10) grams of the dried moringa powder was dissolved in two hundred (200) mL of distilled water and constantly stirred at 60^{o}C on a hotplate for thirty (30) minutes. Once that time had elapsed, the solution was filtered via gravitational deposition, and the top layer of the solution was siphoned and further filtered using filter paper. Twenty (20) mL of the moringa extract was mixed with the 0.33M $AgNO_3$ solution at 60^{o}C for thirty (30) minutes. AgNPs exhibit the phenomena of surface plasmon resonance, which is when electrons become excited by incoming light (Tsuboi et al., 2013). The conducive electrons on the surface will oscillate collectively in resonance with the light's electric field. The Tyndall effect is a phenomenon where particles in a colloidal solution scatter visible light (Huang et al., 2021). By shining a laser through the solution, the visible laser beam is an indication of the AgNPs presence. The solution of AgNPs was centrifuged at 6,000 RPM for two (2) hours, and the supernatant was discarded. The pellet was resuspended in ethanol and left to air dry in a petri dish for approximately two days. The crystalized AgNPs were harvested from the Petri dish and ground in a mortar and pestle to obtain a very fine powder. The powder was weighed to determine the final yield of the biosynthesized nanoparticles from the green synthesis and was stored in a glass vial at 0^{o}C to prevent oxidation. One hundred (100) milligrams of the biosynthesized AgNPs were weighed out on an analytical balance and dissolved in 250 mL of deionized water via sonication. A similar stock solution was prepared using commercial silver nanoparticles that was purchased from the company XFNANO. Confirmation and analysis of the biosynthesized AgNPs was conducted via the use of the Hach DR 6000 UV-VIS (Figure 1A) for ultraviolet spectroscopy and Shimadzu IRSpirit (Figure 1B) for FTIR spectrophotometry. The software, Spectragryph 1.2, was used to analyze the raw infrared spectra of the silver nanoparticles, clean the graph, identify bonds at their respective peak, and conduct corrective measures such as advanced baseline correction in lieu of limitations. The Hach DR 6000 UV-VIS was used to confirm the presence of silver from synthesis.

DOI: 10.31695/IJASRE.2025.10.1

Figure 1. (A) Hach DR 6000 and (B) Shimadzu IRSpirit

PLANT MATERIAL

Cassava (*Manihot esculenta* var. "white") stem cuttings were planted in black soil in *ex vitro* conditions. Approximately ten (10) cassava stem cuttings were planted and irrigated every other day. These represented the mother plants from which explants were obtained for *in vitro* establishment. The systemic fungicide, Python 6.6 SL, was prepared at a concentration of 0.2 % v/v. After approximately two months of growth, the Phyton 6.6 SL solution was applied to the leaves of the cassava plants (Figure 2) every two weeks. This treatment of the cassava plants was carried out for another two (2) months. The plants were kept open to the environment and not under any greenhouse or controlled conditions. Four (4) months after sprouting, young shoots (n = 80) of the cassava plants were excised to be used as initial explants in the establishment phase.

Figure 2. Cassava (*Manihot esculenta* var. "white") plants

INSTRUMENTS

The laboratory work was carried out in sterile conditions. The scalpels and forceps were sterilized in a laboratory oven at 180 °C for 2 hours. The culture media and distilled water were sterilized in a vertical autoclave at 121 °C at 1.2 bar for 30 minutes. During inoculation and subcultures of the explants, the scalpels and forceps were kept inside a Benchmark Microbead Sterilizer at 200^{o}C. The inoculation and transfer operations were carried out at the laminar flow cabinet.

CULTURE MEDIA

The composition of the culture media consisted of full-strength MS Salts and Vitamins. A concentration of 20 g/L of sucrose and 50 mg/L of ascorbic acid was added to the culture media. Since cassava is known to have high levels of polyphenols, it is important to use ascorbic acid as an antioxidant in the culture media to prevent the oxidation of the polyphenols. The pH of the culture media was adjusted to 5.8 with the use of 1.0 M hydrochloric acid (HCl) and/or 1.0 M sodium hydroxide (NaOH) prior to sterilization. The culture media was then gelled with agar at a concentration of 8 g/L.

DOI: 10.31695/IJASRE.2025.10.1

2.2 ESTABLISHMENT PHASE

The plant growth regulators (PGRs) that were used in the establishment phase was the cytokinin, 6-Benzylaminopurine (6-BAP), and the auxin, 1-Naphthaleneacetic acid (NAA), both at a concentration of 1 mg/L. Various concentrations (0, 5, 10, 15, 20 mg/L) of commercial and green AgNPs were studied to determine their effects on the establishment *in vitro* of the cassava explants. Twenty-five (25) mL of culture media were put in each test tube. The explants (10 explants/treatment) were thoroughly washed with water and detergent to initiate the sterilization process. At the laminar flow cabinet, the explants were sterilized in 70% ethanol for ten (10) minutes under constant agitation. Thereafter, they were rinsed three (3) times with sterilized distilled water. The explants were then placed in 3 % Sodium Hypochlorite solution with a drop of TWEEN-20 for twenty (20) minutes under constant agitation. After the time elapsed, the explants were rinsed three (3) times with sterilized distilled water. Using scalpels and forceps, the explants were excised to approximately 2 cm in length and have at least one bud. Prior to inoculation, the mouths of the test tubes were flamed. The forceps were used to place one explant per test tube. The mouth of each test tube was capped then wrapped with saran wrap. The test tubes were placed in the growth room of the Micropropagation Laboratory and kept under controlled conditions of 27 ^{o}C ± 2 with a 12-hour photoperiod. The parameters that were evaluated in this phase include contamination percentage, shoot growth, root growth, and morphological differences.

2.3 DATA ANALYSIS

Data analysis was conducted using the SPSS 16.0 computational statistical package for Windows. The significance level of the tests that were conducted was 5%. Parameters that were assessed include the contamination percentage, shoot growth, and average root length. A two-way Analysis of Variance (ANOVA) was done to determine if there were statistical differences between the different concentrations of AgNPs as well as if there were statistical differences between the commercial and biosynthesized AgNPs. The Tukey HSD test was done to do pairwise comparison between the treatments to determine differences within the groups. The Shapiro-Wilk Test for normality and the Levene's Test was not satisfied hence the reason for the Kruskal-Wallis Test to perform non-parametric analysis of variance.

3. RESULTS AND DISCUSSIONS

3.1 CHARACTERIZATION OF GREEN-SYNTHESIZED SILVER NANOPARTICLES (AgNPs)

The study evaluated the synthesis, characterization, and biological effects of green AgNPs derived from *Moringa oleifera* extract, comparing them with commercial AgNPs.

UV-VIS AND FTIR ANALYSIS

The UV-VIS and FTIR analyses of the green-synthesized nanoparticles using *Moringa oleifera* powder provide critical insights into the synthesis mechanism, nanoparticle formation, and the role of phytochemicals. The UV-VIS spectrum revealed absorption peaks at 240 nm and 304 nm, which deviate from the typical surface plasmon resonance (SPR) band of silver nanoparticles (AgNPs) observed at 400–450 nm. This anomaly can be attributed to several factors. Moringa extract contains aromatic compounds (e.g., flavonoids, phenolic acids) that absorb strongly in the UV range (200–300 nm) as seen in Figure 3. The peak at 240 nm likely corresponds to $\pi \rightarrow \pi^*$ transitions in conjugated systems, such as quercetin or chlorogenic acid, which are abundant in Moringa. The 304 nm peak may indicate the

DOI: 10.31695/IJASRE.2025.10.1

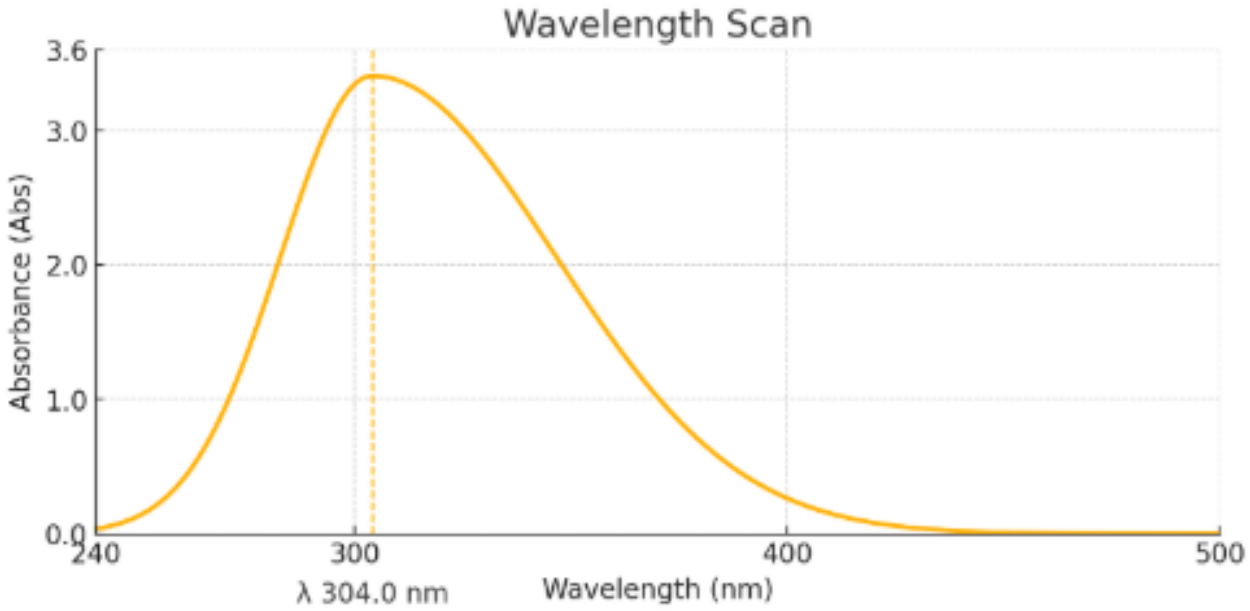

Figure 3. UV-Vis of Green Nanoparticles coated with Moringa extract with peak absorption at 304 nm

formation of ultra-small AgNPs (<10 nm). Smaller nanoparticles exhibit blue-shifted SPR bands due to quantum confinement effects (Ugwoke et al., 2019; Bindhu et al., 2020). However, the absence of a distinct SPR peak in the visible range suggests partial aggregation or masking by organic capping agents. The dense phytochemical matrix of Moringa could scatter light, obscuring the SPR signal. This is common in biogenic synthesis where organic residues dominate the optical profile.

The FTIR transmission data (wavenumbers 4000–400 cm^{-1}) identifies key functional groups in Moringa involved in nanoparticle reduction and stabilization as seen in Figure 4. Broad dips in the 3200–3600 cm^{-1} region suggest the presence of hydroxyl groups from polyphenols, alcohols, or water. This is known as the O-H Stretching region. These groups reduce Ag^{+} ions via electron donation (Moodley et al., 2018; Pratiwi et al. 2019). Carbonyl stretching in the

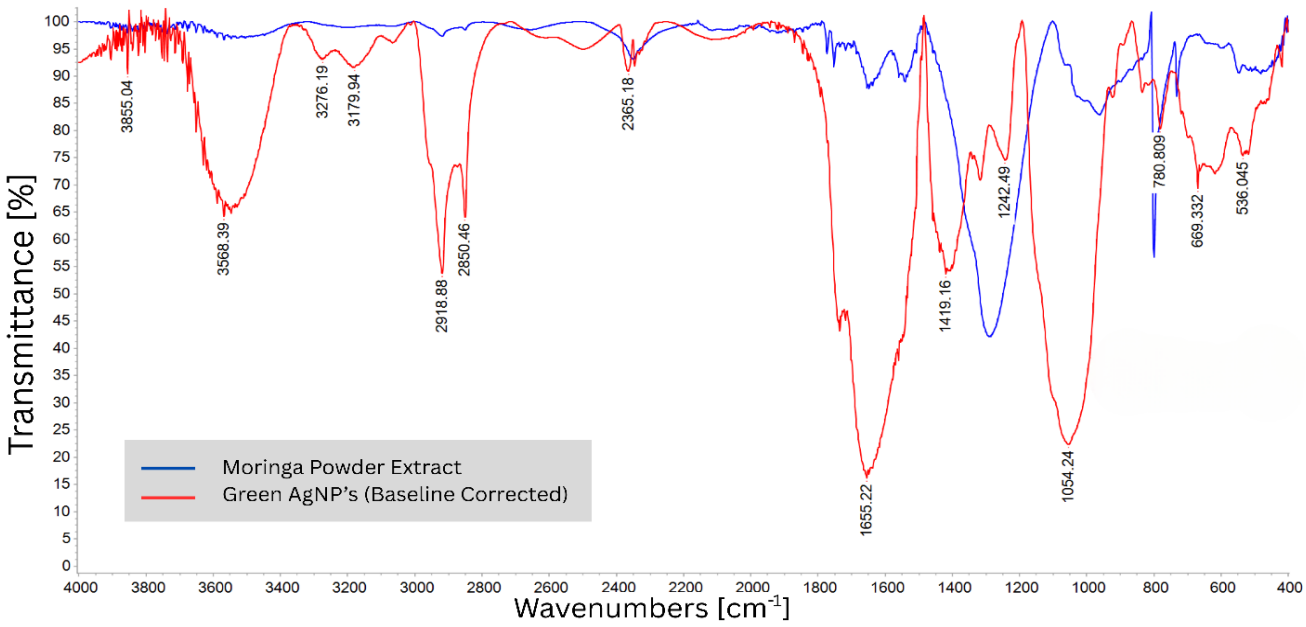

Figure 4. FTIR graph comparing Moringa powder analysis versus Silver ions coated in Moringa extract

DOI: 10.31695/IJASRE.2025.10.1

1600–1700 cm^{-1} region indicates carbonyl groups from proteins or ketones, which stabilize nanoparticles by forming coordination bonds with Ag^{+}. C-O-C and C-N Stretching (1000–1300 cm^{-1}) in this range correspond to polysaccharides or amine groups, further confirming the role of Moringa biomolecules in capping AgNPs. Hydroxyl (-OH) and carbonyl (-C=O) groups donate electrons to reduce Ag^{+} to Ag^{0}, initiating nucleation. Proteins and polysaccharides adsorb onto nanoparticle surfaces, preventing aggregation via steric or electrostatic stabilization (Isah et al., 2022). The absence of a strong SPR band in UV-VIS may reflect incomplete reduction or dominance of organic chromophores. However, the FTIR confirmation of reducing/capping agents aligns with successful nanoparticle formation, as reported in similar studies using plant extracts.

3.2 EFFECTS OF AgNPs ON SHOOT AND ROOT DEVELOPMENT

SHOOT LENGTH

In commercial AgNPs treatments, a one-way ANOVA revealed a significant effect of concentration on shoot length ($F(4, 245) = 5.30$, $p = 0.0004$). Post-hoc Tukey's HSD indicated that shoots at 15 mg/L (Treatment 4; M = 1.822 cm, SD = 3.27) and 20 mg/L (Treatment 5; M = 1.687 cm, SD = 1.97) were significantly longer than the control as seen in Figure 5 (Treatment 1; M = 0.12 cm, SD = 0.41).

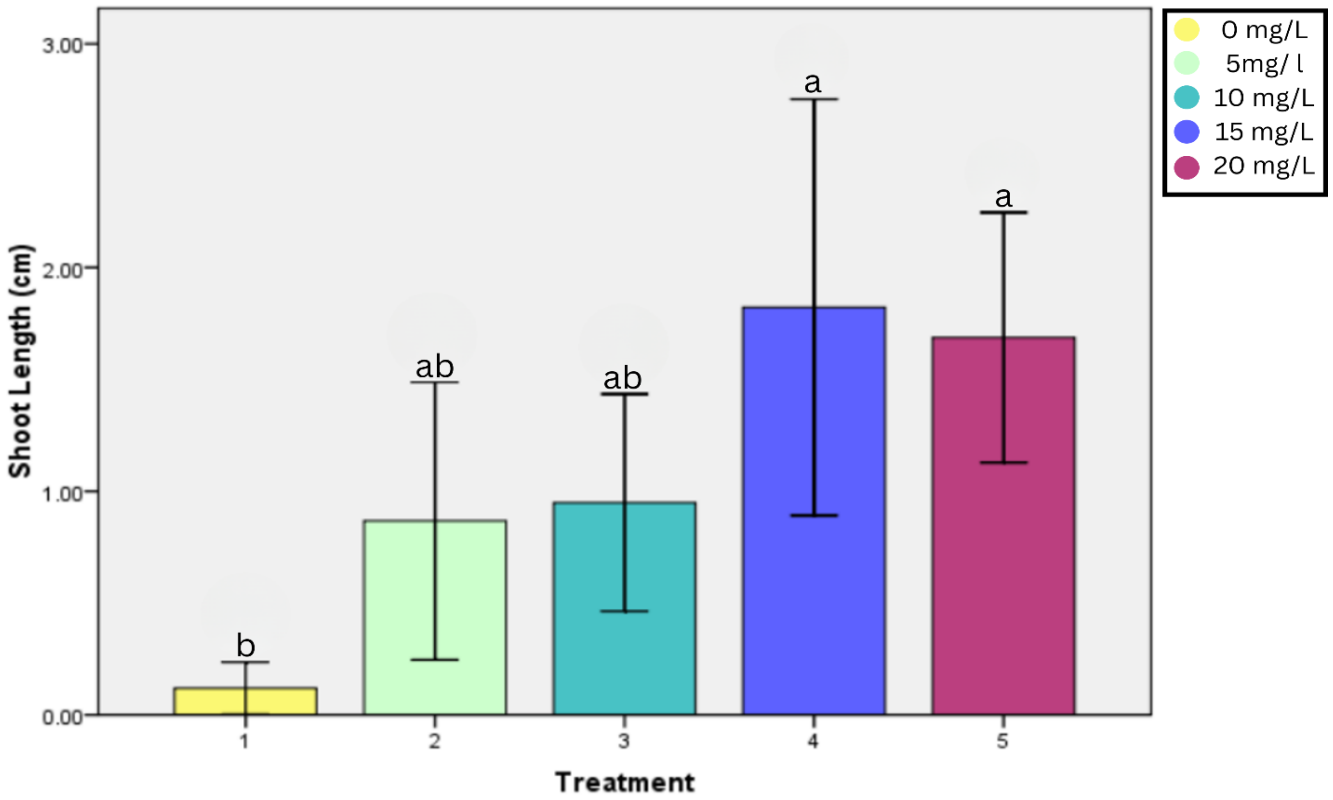

Means with different letters differ statistically for $p<0.05$ according to Two-way ANOVA (Tukey HSD).

Figure 5. Average shoot length (cm) in Commercial AgNPs across treatments 0, 5, 10, 15, 20 mg/L (Treatments 1-5)

In green-synthesized AgNPs treatments, shoot length also varied significantly across concentrations ($F (4, 245) = 11.43$, $p < 0.001$). Tukey's HSD tests showed that control shoots (M = 2.20 cm, SD = 3.70) were significantly longer than all other treatments (5–20 mg/L), which exhibited reduced elongation (e.g., Treatment 2: M = 0.38 cm, SD = 1.19).

DOI: 10.31695/IJASRE.2025.10.1

Because some treatment groups violated normality (Shapiro–Wilk $p < 0.05$) and homogeneity of variance (Levene's test $p < 0.05$), the two-way ANOVA was complemented with Kruskal–Wallis and Dunn's post-hoc tests to compare median shoot lengths across the five concentration treatments. A Kruskal–Wallis H test revealed a highly significant difference in shoot length distributions among the five commercial AgNPs concentration groups ($H(4) = 44.65$, $p < 0.001$, $\eta^2 = 0.17$), indicating that not all medians were equal. Pairwise Dunn's tests with Bonferroni correction identified four significant differences in median shoot length, which were between pairs 1 vs 3, 1 vs 5, 2 vs 3, and 2 vs 5. For green-synthesized AgNPs, the Kruskal–Wallis test also showed significant differences across treatments as seen in Figure 6 ($H(4) = 32.78$, $p < 0.001$, $\eta^2 = 0.12$). The subsequent Dunn's tests (Bonferroni-adjusted) indicated significant median differences between the control and all the other treatments.

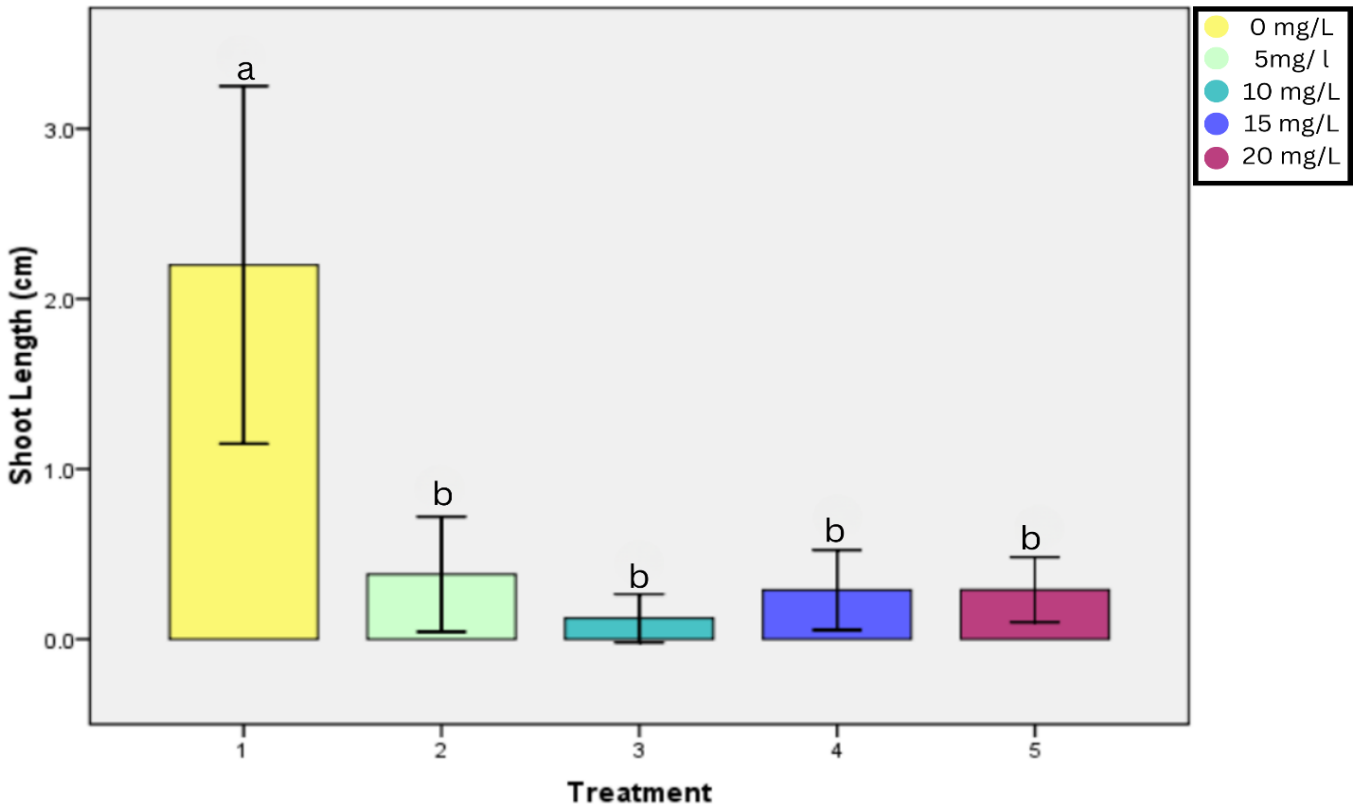

Means with different letters differ statistically for p<0.05 according to a Two-way ANOVA (Tukey HSD).

Figure 6. Average shoot length (cm) in Green AgNPs across treatments 0, 5, 10, 15, 20 mg/L (Treatments 1-5)

The divergent outcomes of commercial and green AgNPs stem from fundamental differences in their synthesis, stability, and surface chemistry. Commercial AgNPs are typically synthesized via chemical reduction using citrate as a stabilizing agent. Citrate confers a negative surface charge (zeta potential ≈ -30 mV), preventing aggregation and ensuring uniform dispersion in aqueous media (Park & Lee, 2013). This stability enables sustained release of Ag^+ ions, which modulate plant physiological processes at subtoxic thresholds (Pokhrel et al., 2013; Gontijo et al., 2020). At 15–20 mg/L, the gradual Ag^+ release likely achieves a hormetic balance that is sufficient to suppress microbial competitors, but insufficient to induce oxidative damage. Green synthesis using *Moringa oleifera* extract introduces biomolecules such as flavonoids and alkaloids that reduce Ag^+ ions and cap nanoparticles. While this "green" approach avoids harsh chemicals, residual phytochemicals adsorbed onto AgNPs alter their behavior (Nasiri et al., 2018). For instance, phenolic compounds in Moringa can chelate metal ions, reducing Ag^+ bioavailability. Concurrently, these organics may act as Trojan horses, facilitating nanoparticle internalization while delivering phytotoxic secondary metabolites. The result is a dual stressor causing Ag^+-induced ROS and direct inhibition by plant-derived compounds (Shaikhaldein et al., 2020).

DOI: 10.31695/IJASRE.2025.10.1

Nanoparticle entry into plant cells dictates their bioactivity. Commercial and green AgNPs likely follow distinct uptake pathways due to differences in size, charge, and surface coatings. Citrate-stabilized AgNPs (10–20 nm diameter) primarily enter roots via apoplastic flow, traversing cell walls without membrane interaction. However, in shoot tissues, their smaller size may enable endocytic uptake (Quevedo et al., 2021). Once internalized, Ag^+ ions disrupt Ca^{2+} signaling, a critical regulator of cell elongation. At optimal concentrations (15–20 mg/L), this disruption may enhance calcium-dependent kinase activity, promoting mitosis in shoot meristems (Syu et al., 2014). The organic corona of green AgNPs increases hydrophobicity, favoring membrane adhesion and fluid-phase endocytosis. Once inside cells, nanoparticles localize to vacuoles and chloroplasts, where acidic conditions accelerate Ag^+ release (Ramasamy et al., 2024). Chloroplastic accumulation is particularly detrimental, as Ag^+ interferes with photosystem II (PSII) electron transport, reducing ATP synthesis and stunting shoot growth (Štefanić et al., 2021). This explains the drastic shoot inhibition even at 5 mg/L of green AgNPs as seen in Figure 7. Ag^+ ions structurally resemble cytokinins, enabling them to bind cytokinin receptors. This mimicry upregulates ARR (response regulator) genes, stimulating cell division in shoot apical meristems (Nartop, 2022). Concurrently, Ag^+ inhibits ethylene biosynthesis by blocking ACC oxidase, an enzyme critical for ethylene production. Ethylene typically restricts shoot elongation. Its suppression thus synergizes with cytokinin signaling to promote growth at 15–20 mg/L (Paladi et al., 2017). The Moringa-derived compounds on green AgNPs may antagonize auxin transport. Auxin efflux carriers (PIN proteins) are sensitive to oxidative stress, which green AgNPs exacerbate via ROS overproduction. Additionally, phenolic compounds like quercetin in Moringa inhibit polar auxin transport (PAT) (Naseem & Dandekar, 2012), disrupting apical dominance. Compounding this, green AgNPs trigger jasmonate synthesis—a stress hormone that antagonizes cytokinins. The net result is a collapse in meristematic activity, manifesting as stunted shoots across all concentrations. In peach, shoot

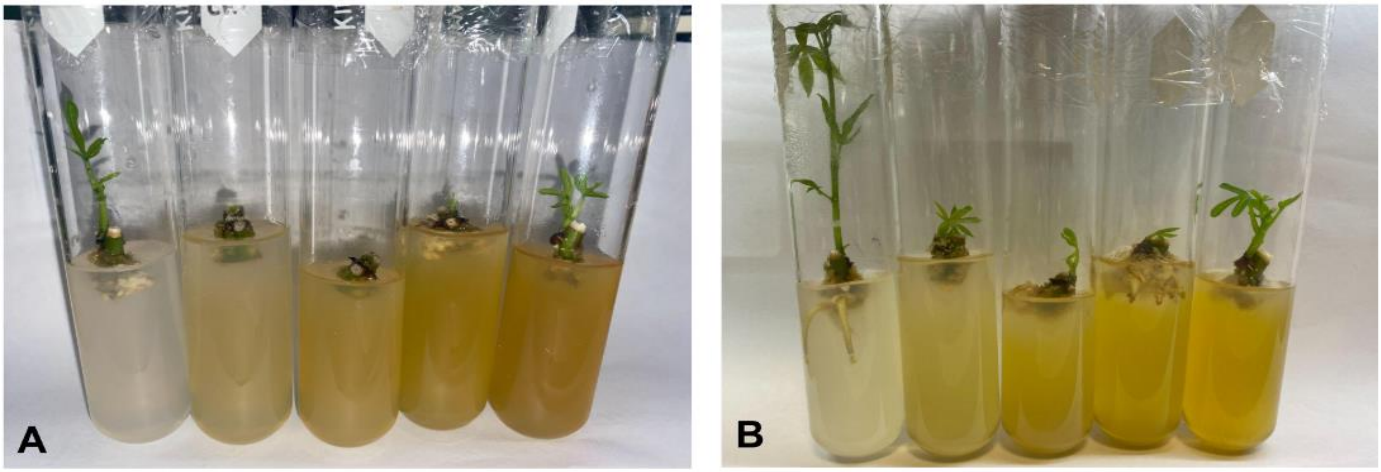

Figure 7. Shoot Development A. (Left to right) 0, 5, 10, 15, 20 mg/L in week 2. B. (Left to right) 0, 5, 10, 15, 20 mg/L in week 3 in Green Silver Nanoparticles

elongation defects were associated with downregulation of auxin and cytokinin signaling and upregulation of jasmonic acid and stress-related genes, paralleling the phytotoxic effects observed with green AgNPs (Lian et al., 2020). A hormonal cascade involving jasmonic acid, ethylene, and abscisic acid was shown to restrict shoot growth in *Ricinus communis*, offering a model for how green AgNP-induced stress responses might work (Veselov et al., 2003).

Reactive oxygen species (ROS) plays paradoxical roles. At low levels, they act as signaling molecules while at high levels, they induce cellular damage. At 15–20 mg/L, commercial AgNPs enhance catalase (CAT) and superoxide dismutase (SOD) activity, as shown in wheat seedlings. This antioxidant upregulation neutralizes ROS generated during normal metabolism, creating a redox environment conducive to growth (Rastogi et al., 2018). Citrate itself may contribute by chelating free Fe^{2+}, preventing Fenton reactions (Grzelak et al., 2018). Green AgNPs induce a ROS "burst" through multiple pathways. Ag^+-induced Ca^{2+} influx activates membrane-bound NADPH oxidases, generating superoxide (O_2^-). Exposure to AgNPs triggers oxidative stress through Ca^{2+}-dependent NADPH oxidase activation and ROS amplification. This overwhelms the cellular redox buffering systems, leading to lipid peroxidation, DNA damage, and protein carbonylation (He et al., 2024; Lee et al., 2024). Chloroplast leakage occurs due to PSII

DOI: 10.31695/IJASRE.2025.10.1

disruption, which releases singlet oxygen ($^1O_2$), which then peroxidizes lipids in thylakoid membranes. AgNPs impair PSII activity in wheat and aquatic plants, leading to singlet oxygen ($^1O_2$) production and membrane lipid peroxidation—hallmarks of chloroplast-origin ROS damage (Jiang et al., 2017). Ag^+ uncouples electron transport chains, increasing H_2O_2 production, which causes mitochondrial dysfunction. AgNPs disrupt mitochondrial function, increasing mitochondrial ROS and damaging proteins through sulfenylation. This results in oxidative stress-induced cell cycle arrest and apoptosis in plant and animal models (Holmila et al., 2019).

ROOT LENGTH

For commercial AgNPs, root length differed significantly among treatments ($F(4, 245) = 5.41$, $p = 0.0003$). Tukey's HSD identified that Treatment 3 (10 mg/L; M = 0.44 cm, SD = 0.90) and Treatment 4 (15 mg/L; M = 0.38 cm, SD = 0.98) produced significantly longer roots than the control (0 mg/L; M = 0.00 cm). Green AgNPs also had a significant effect on root length ($F(4, 245) = 5.73$, $p = 0.0002$). Post-hoc analysis showed that control roots (M = 0.76 cm, SD = 1.57) were longer than those at all other concentrations, with the greatest inhibition observed at 5 mg/L (Treatment 2;

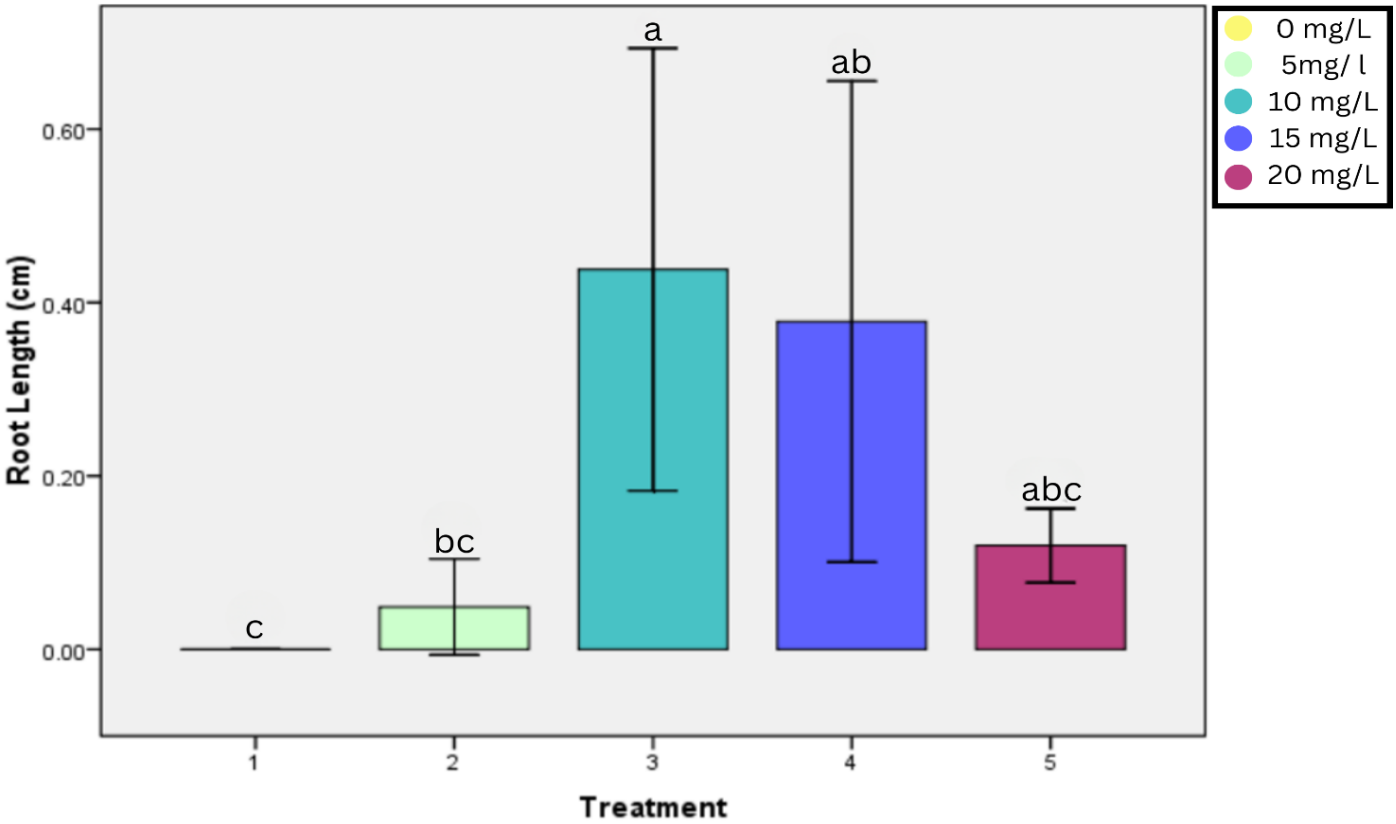

Means with different letters differ statistically for $p<0.05$ according to a Two-way ANOVA (Tukey HSD).

Figure 8. Average root length (cm) in Commercial AgNPs across treatments 0, 5, 10, 15, 20 mg/L (Treatments 1-5)

M = 0.07 cm, SD = 0.26). To account for violations of normality and homogeneity of variance in the root-length data (Shapiro–Wilk and Levene's tests both $p < 0.05$), Kruskal–Wallis H-tests followed by Dunn's post-hoc comparisons (Bonferroni-adjusted) were performed for each AgNP source (Figure 8). No other pairwise differences reached statistical significance. For green AgNPs, the Kruskal–Wallis test likewise revealed a significant treatment effect on median root length ($H(4) = 33.93$, $p < 0.001$). Dunn's post-hoc comparisons showed that the control group (0 mg/L) differed significantly from 5 mg/L ($z = 3.6612$, $p\_adj = 0.0025$), 10 mg/L ($z = 3.0091$, $p\_adj = 0.0262$), and 20 mg/L ($z = 3.5291$, $p\_adj = 0.0042$), indicating pronounced inhibition at those concentrations. Other pairwise contrasts were not significant, as seen in Figure 9.

DOI: 10.31695/IJASRE.2025.10.1

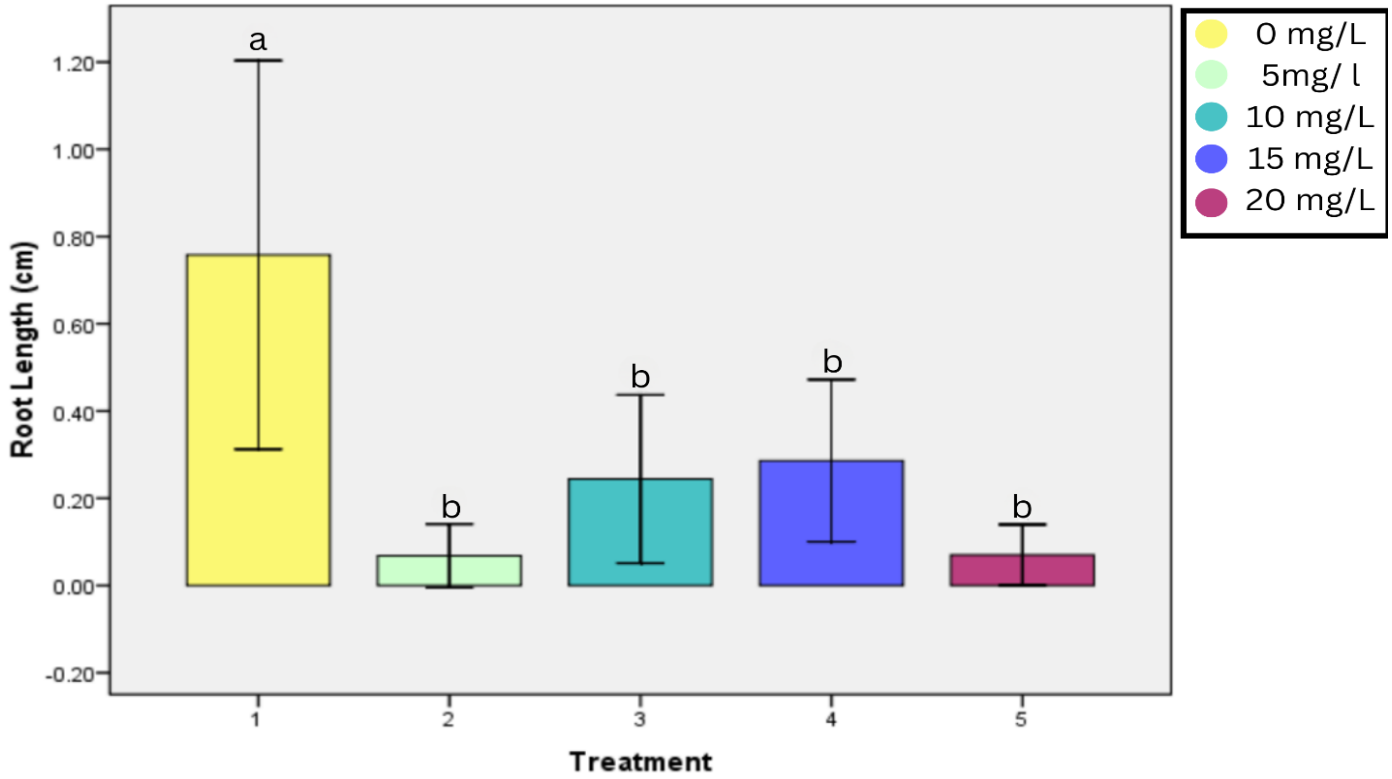

Means with different letters differ statistically for $p<0.05$ according to a Two-way ANOVA (Tukey HSD).

Figure 9. Average root length (cm) in Green AgNPs across treatments 0, 5, 10, 15, 20 mg/L (Treatments 1-5)

Root development is governed by auxin-ethylene balance, with cytokinins playing a modulatory role. AgNPs disrupt this equilibrium through direct and indirect mechanisms. Ag^+ ions released from commercial AgNPs inhibit ACC oxidase, a key enzyme in ethylene biosynthesis (Syu et al., 2014). Ethylene normally restricts root elongation by promoting radial expansion. Its suppression at 10–15 mg/L likely shifts growth toward longitudinal cell division as seen in Figure 8.

Concurrently, Ag^+ stabilizes auxin efflux carriers (PIN proteins) by interacting with sulfhydryl groups, enhancing auxin polar transport to root tips (Zhao & Hasenstein, 2009). Green AgNPs coated with phytochemicals (e.g., quercetin) disrupt auxin accumulation and signaling. For instance, AgNPs reduced auxin receptor gene expression (TIR1/AFB family) and impaired gravitropism in Arabidopsis, a phenotype tied to faulty auxin transport (Sun et al., 2017). Additionally, green AgNPs induce jasmonic acid (JA) synthesis, a stress hormone that suppresses root meristem activity by downregulating PLETHORA genes. The result is stunted root growth across all concentrations, with the strongest inhibition at 5 mg/L (M = 0.07 cm), where nanoparticle uptake is maximized without aggregation (Lewis et al., 2011; Lian et al., 2020).

Root and shoot development after two and three weeks of culture with commercial nanoparticles can be seen in Figure 10. Nanoparticle entry routes and intracellular fate critically determine phytotoxicity. Citrate-stabilized commercial AgNPs primarily traverse the apoplast, avoiding symplastic uptake. Those entering cells via endocytosis are sequestered in vacuoles, where acidic pH (≈5.5) slows Ag^+ release (Hudecova et al., 2012; Butler et al., 2015). This compartmentalization limits cytoplasmic toxicity, allowing roots to tolerate higher doses (15 mg/L: M = 0.38 cm). The hydrophobic surface of green AgNPs facilitates membrane adhesion and fluid-phase endocytosis. Once internalized, nanoparticles accumulate in mitochondria and nuclei, where Ag^+ directly binds DNA, forming Ag-DNA adducts, and disrupts ATP synthesis (Baldi et al., 2016). Mitochondrial targeting explains the acute toxicity even at 5 mg/L (M = 0.07 cm), as energy deficits impair root hair formation and meristematic activity.

DOI: 10.31695/IJASRE.2025.10.1

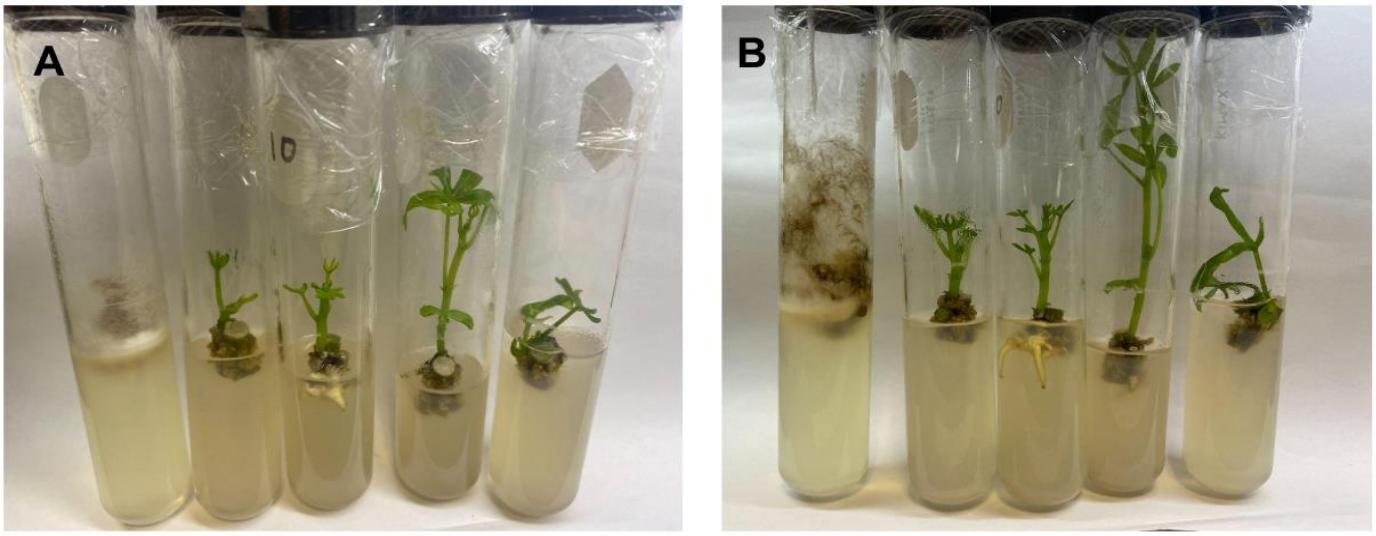

Figure 10. Root & shoot Development A. (Left to right) 0, 5, 10, 15, 20 mg/L in week 2. B. (Left to right) 0, 5, 10, 15, 20 mg/L in week 3 in Commercial Silver Nanoparticles

MORPHOLOGICAL ABNORMALITIES

In both concentrations (10 mg/L and 15 mg/L), the cassava cuttings displayed abnormal root morphology. The roots appear swollen, short, and thickened, with a somewhat callus-like or lignified appearance, especially at 15 mg/L (Figure 11). The swollen, thickened roots suggest aberrant cell expansion or proliferation, potentially triggered by oxidative stress or phytohormonal disruption. Green AgNPs may interfere with auxin transport or signaling, which is critical for root elongation. Auxin mis-regulation often leads to root tip swelling or callus formation, mimicking mature root tissues prematurely.

In apple rootstocks, silver nanoparticles loaded with indole-3-acetic acid (IAA) caused excessive callus formation and abnormal root morphology, implicating auxin overstimulation or misrouting (Korpayev et al., 2021). Green AgNPs, rich in phytochemicals like flavonoids and alkaloids, might act as signaling mimics or toxins, inducing pathways associated with secondary growth or tuberization. In wheat roots, exposure to ≥5 ppm AgNPs led to lignin and callose deposition, visible swelling, and ROS-induced ultrastructural changes. This supports early differentiation and defense responses such as suberization (Yanık & Vardar, 2019). The root phenotype resembling mature cassava storage roots could also be a form of premature differentiation, possibly driven by jasmonic acid induction or disrupted cytokinin/auxin ratios, both of which are influenced by nanoparticle exposure. This suggests that the green AgNPs are not only inhibiting meristematic activity, but may also be redirecting developmental programs toward storage root pathways in a disorganized way (Wang et al., 2019).

DOI: 10.31695/IJASRE.2025.10.1

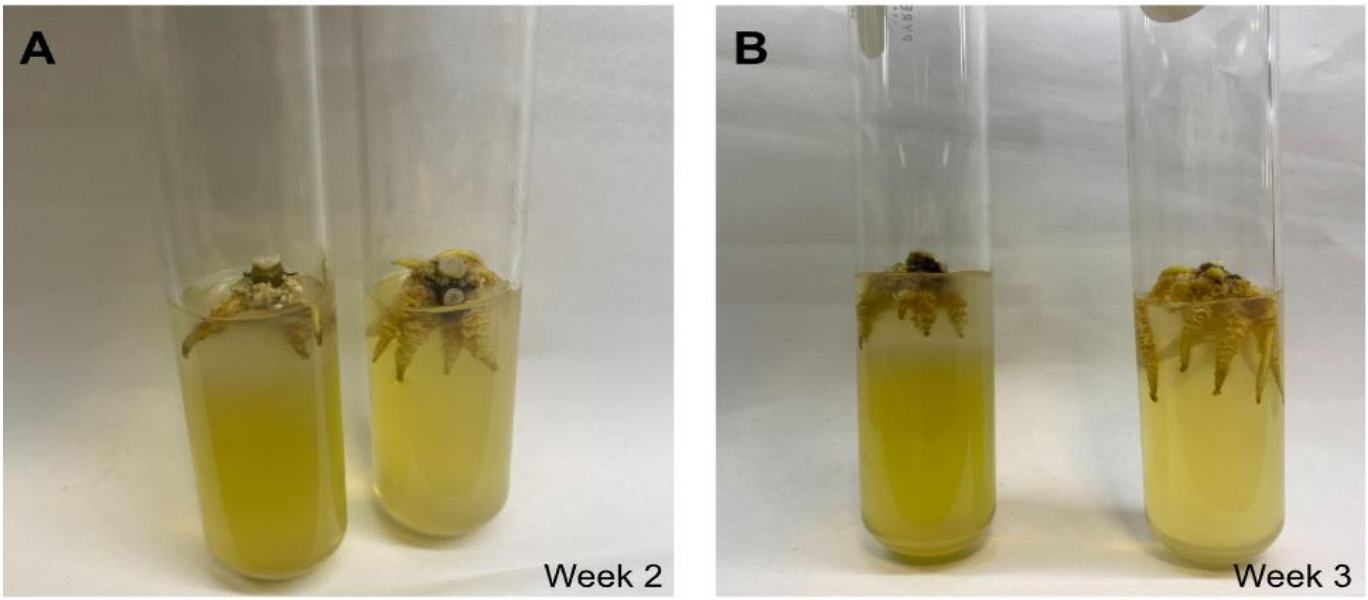

Figure 11. Root Development A. (Left test tube) 10 mg/L vs (Right test tube) 15 mg/L for Green Nanoparticles in week 2. B (Left test tube) 10 mg/L vs (Right test tube) 15 mg/L in week 3.

ANTIMICROBIAL EFFICACY AND CONTAMINATION RATES

Contamination rates indirectly influence root development by altering nutrient availability and hormone synthesis. At 20 mg/L, commercial AgNPs reduce contamination to 10%, minimizing microbial competition for sucrose and micronutrients. Uninfected roots allocate more resources to growth, while suppressed ethylene-producing microbes (e.g., Pseudomonas) further enhance elongation. The 80% contamination rate at 15 mg/L green AgNPs (Table 1) suggests microbial adaptation to organic capping agents. Moringa phenolics may serve as carbon sources for fungi (e.g., Fusarium), which secrete ethylene precursors (ACC) and phytotoxins (e.g., fusaric acid). This exacerbates root inhibition, particularly at 5 mg/L, where nanoparticle antimicrobial efficacy is lowest (Fayyadh et al., 2024).

Contamination percentages between commercial and green AgNP treatments were compared to evaluate antimicrobial efficacy. Contamination was scored as the percentage of explants exhibiting microbial growth after four weeks. As shown in Table 1, green AgNPs at 15 mg/L (Treatment 4) exhibited the highest contamination (80 ± 0.0 %), whereas commercial AgNPs at 20 mg/L (Treatment 5) achieved the lowest contamination (10 ± 0.0 %).

Table 1. Contamination rates (%) for commercial vs. green AgNPs treatments.

Treatment	Commercial AgNPs (%)	Green AgNPs (%)
1 (0 mg/L)	66.0 ± 13.4^{c}	24.0 ± 32.9^{a}
2 (5 mg/L)	34.0 ± 8.9^{b}	24.0 ± 30.9^{a}
3 (10 mg/L)	42.0 ± 8.4^{b}	48.0 ± 30.3^{ab}
4 (15 mg/L)	28.0 ± 4.5^{b}	80.0 ± 0.0^{b}
5 (20 mg/L)	10.0 ± 0.0^{a}	64.0 ± 16.7^{ab}

Means with different letters within the column differ statistically for $p<0.05$ according to a Two-way ANOVA (Tukey HSD).

DOI: 10.31695/IJASRE.2025.10.1

Silver nanoparticles reduce microbial contamination in tissue cultures, improving explant health and growth. In banana cultures, AgNPs significantly suppressed endophytic and surface contaminants, allowing for better nutrient availability and shoot development (Nazir et al., 2023). AgNPs suppress ethylene production, which further promotes shoot elongation. Sub-lethal AgNP concentrations in tobacco tissue culture reduced ethylene biosynthetic gene expression (ACS2) and enhanced growth by downregulating key ethylene signaling components (e.g., ETR1, ERS1, CTR1) (Sarmast & Salehi, 2021). Endophyte suppression may limit excess auxin production, benefiting shoot development. Certain endophytes are known to overproduce indole-3-acetic acid (IAA), which can disrupt shoot-to-root hormonal balance (Korpayev et al., 2021). Microbial persistence despite green AgNP exposure has been reported. Organic capping agents from green synthesis may serve as carbon sources for fungi like Fusarium, worsening contamination in tissue cultures (Ahlawat et al., 2020). Pathogens like Fusarium secrete ethylene precursors (e.g., ACC) and mycotoxins (e.g., fusaric acid), which disrupt hormone signaling and further suppress shoot elongation (Fayyadh et al., 2024). Silver nanoparticles significantly reduced contamination in *Tecomella undulata* tissue culture and enhanced shoot proliferation, likely due to ethylene inhibition and nutrient preservation (Aghdaei et al., 2013).

CONCLUSIONS

Green-synthesized silver nanoparticles (AgNPs), produced via *Moringa oleifera* extract were successfully synthesized and characterized. The UV–VIS and FTIR analyses confirmed the formation of AgNPs, with characteristic surface-plasmon absorption features and phytochemical capping by moringa biomolecules. Commercial AgNPs significantly enhanced shoot length at 15–20 mg/L (ANOVA $F(4, 245)=5.30$, $p=0.0004$) and increased median root length at 20 mg/L ($z=-4.39$, $p<0.001$). In contrast, green-synthesized AgNPs inhibited both shoot and root elongation across all concentrations and induced morphological abnormalities—such as swollen, callus-like roots—indicative of phytotoxic stress. Commercial AgNPs at 20 mg/L yielded the lowest contamination (10 %), whereas green AgNPs at 15 mg/L had the highest (80 %), demonstrating that the biogenic particles, as currently prepared, offer limited microbial suppression. Overall, while commercial AgNPs met both antimicrobial and growth-promotion roles, the green-synthesized AgNPs only satisfied the synthesis objective.

BIBLIOGRAPHY

1. Aghdaei, M., Salehi, H., & Sarmast, M. (2013). Effects of silver nanoparticles on Tecomella undulate (Roxh.) Seem. Micropropagation. DOAJ (DOAJ: Directory of Open Access Journals). https://doi.org/10.13128/ahs-12748

2. Ahlawat, J., Sehrawat, A., Choudhary, R., & Yadav, S. (2020). Biologically synthesized silver nanoparticles eclipse fungal and bacterial contamination in micropropagation of Capparis decidua (FORSK.) Edgew: A substitute to toxic substances. Indian Journal of Experimental Biology, 58(5). https://doi.org/10.56042/ijeb.v58i05.65485

3. Alfarraj, N. S., Tarroum, M., Al-Qurainy, F., Nadeem, M., Khan, S., Salih, A. M., Shaikhaldein, H. O., Al-Hashimi, A., Alansi, S., & Perveen, K. (2023). Biosynthesis of Silver Nanoparticles and Exploring Their Potential of Reducing the Contamination of the In Vitro Culture Media and Inducing the Callus Growth of Rumex nervosus Explants. Molecules, 28(9), 3666. https://doi.org/10.3390/molecules28093666

4. Baldi, F., Daniele, S., Gallo, M., Paganelli, S., Battistel, D., Piccolo, O., Faleri, C., Puglia, A. M., & Gallo, G. (2016). Polysaccharide-based silver nanoparticles synthesized by Klebsiella oxytoca DSM 29614 cause DNA fragmentation in E. coli cells. BioMetals, 29(2), 321–331. https://doi.org/10.1007/s10534-016-9918-4

5. Bindhu, Umadevi, M., Esmail, G. A., Al-Dhabi, N. A., & Arasu, M. V. (2020). Green synthesis and characterization of silver nanoparticles from Moringa oleifera flower and assessment of antimicrobial and sensing properties. Journal of Photochemistry and Photobiology B Biology, 205, 111836. https://doi.org/10.1016/j.jphotobiol.2020.111836

DOI: 10.31695/IJASRE.2025.10.1

6. Butler, K. S., Peeler, D. J., Casey, B. J., Dair, B. J., & Elespuru, R. K. (2015). Silver nanoparticles: correlating nanoparticle size and cellular uptake with genotoxicity. Mutagenesis, 30(4), 577–591. https://doi.org/10.1093/mutage/gev020

7. Chavez, V. A., Milne, A. E., Van Den Bosch, F., Pita, J., & McQuaid, C. F. (2021). Modelling cassava production and pest management under biotic and abiotic constraints. Plant Molecular Biology, 109(3), 325–349. https://doi.org/10.1007/s11103-021-01170-8

8. Courtois, P., Rorat, A., Lemiere, S., Guyoneaud, R., Attard, E., Levard, C., & Vandenbulcke, F. (2019). Ecotoxicology of silver nanoparticles and their derivatives introduced in soil with or without sewage sludge: A review of effects on microorganisms, plants and animals. Environmental Pollution, 253, 578–598. https://doi.org/10.1016/j.envpol.2019.07.053

9. FAOSTAT Analytical Briefs. (2023). Agricultural production statistics 2000–2022. In FAO. https://doi.org/10.4060/cc9205en

10. Fayyadh, M. A., Manea, A. A., & Salih, Y. A. (2024). Molecular Identification of Fusarium Species Associated with the Tissue Culture Date Palm Offshoots Wilt Disease and Evaluation of Using Silver Nanoparticles and Trichoderma longibrachiatum for Its Control. *Arab Journal of Plant Protection*, *42*(2), 189–195. https://doi.org/10.22268/ajpp-001225

11. Gontijo, L. a. P., Raphael, E., Ferrari, D. P. S., Ferrari, J. L., Lyon, J. P., & Schiavon, M. A. (2020). pH effect on the synthesis of different size silver nanoparticles evaluated by DLS and their size-dependent antimicrobial activity. Matéria (Rio De Janeiro), 25(4). https://doi.org/10.1590/s1517-707620200004.1145

12. Grün, A., & Emmerling, C. (2018). Long-term effects of environmentally relevant concentrations of silver nanoparticles on major soil bacterial phyla of a loamy soil. Environmental Sciences Europe, 30(1). https://doi.org/10.1186/s12302-018-0160-2

13. Grzelak, A., Wojewódzka, M., Meczynska-Wielgosz, S., Zuberek, M., Wojciechowska, D., & Kruszewski, M. (2018). Crucial role of chelatable iron in silver nanoparticles induced DNA damage and cytotoxicity. Redox Biology, 15, 435–440. https://doi.org/10.1016/j.redox.2018.01.006

14. He, J., Ma, Y., Niu, X., Pei, J., Yan, R., Xu, F., Ma, J., Ma, X., Jia, S., & Ma, W. (2024). Silver nanoparticles induce endothelial cytotoxicity through ROS-mediated mitochondria-lysosome damage and autophagy perturbation: The protective role of N-acetylcysteine. Toxicology, 502, 153734. https://doi.org/10.1016/j.tox.2024.153734

15. Holmila, R. J., Vance, S. A., Singh, R., King, S. B., & Furdui, C. M. (2019). Abstract 887: Silver nanoparticles and ionizing radiation induce mitochondrial protein oxidation and effects on cell cycle and proliferation in lung cancer cell lines. Cancer Research, 79(13_Supplement), 887. https://doi.org/10.1158/1538-7445.am2019-887

16. Hossain, Z., Mustafa, G., & Komatsu, S. (2015). Plant responses to nanoparticle stress. International Journal of Molecular Sciences, 16(11), 26644–26653. https://doi.org/10.3390/ijms161125980

17. Huang, J., Mo, X., Fu, H., Sun, Y., Gao, Q., Chen, X., Zou, J., Yuan, Y., Nie, J., & Zhang, Y. (2021). Tyndall-effect-enhanced supersensitive naked-eye determination of mercury (II) ions with silver nanoparticles. Sensors and Actuators B Chemical, 344, 130218. https://doi.org/10.1016/j.snb.2021.130218

18. Hudecova, A., Kusznierewicz, B., Runden-Pran, E., Magdolenova, Z., Hasplova, K., Rinna, A., Fjellsbo, L. M., Kruszewski, M., Lankoff, A., Sandberg, W. J., Refsnes, M., Skuland, T., Schwarze, P., Brunborg, G., Bjoras, M., Collins, A., Miadokova, E., Galova, E., & Dusinska, M. (2012). Silver nanoparticles induce premutagenic DNA

DOI: 10.31695/IJASRE.2025.10.1

oxidation that can be prevented by phytochemicals from Gentiana asclepiadea. Mutagenesis, 27(6), 759–769. https://doi.org/10.1093/mutage/ges046

19. Isah, M., Ayuba, S., & Bello, Z. (2022). Antioxidant and antimicrobial activities of green synthesized silver nanoparticle using Moringa oleifera seeds extracts. Caliphate Journal of Science and Technology, 4(2), 142–150. https://doi.org/10.4314/cajost.v4i2.3

20. Jiang, H. S., Yin, L. Y., Ren, N. N., Zhao, S. T., Li, Z., Zhi, Y., Shao, H., Li, W., & Gontero, B. (2017). Silver nanoparticles induced reactive oxygen species via photosynthetic energy transport imbalance in an aquatic plant. Nanotoxicology, 11(2), 157–167. https://doi.org/10.1080/17435390.2017.1278802

21. Kalwar, K., & Shan, D. (2018) Antimicrobial effect of silver nanoparticles (AgNPs) and their mechanism – a mini review. Micro & Nano Letters, 13(3), 277–280. https://doi.org/10.1049/mnl.2017.0648

22. Korpayev, S., Karakeçili, A., Dumanoğlu, H., & Osman, S. I. A. (2021). Chitosan and silver nanoparticles are attractive auxin carriers: A comparative study on the adventitious rooting of microcuttings in apple rootstocks. Biotechnology Journal, 16(8). https://doi.org/10.1002/biot.202100046

23. Lee, C., Wang, F., Huang, C., & Chan, W. (2024). Dose-dependent effects of silver nanoparticles on cell death modes in mouse blastocysts induced via endoplasmic reticulum stress and mitochondrial apoptosis. Toxicology Research, 13(5). https://doi.org/10.1093/toxres/tfae158

24. Lewis, D. R., Negi, S., Sukumar, P., & Muday, G. K. (2011). Ethylene inhibits lateral root development, increases IAA transport and expression of PIN3 and PIN7 auxin efflux carriers. Development, 138(16), 3485–3495. https://doi.org/10.1242/dev.065102

25. Lian, X., Tan, B., Yan, L., Jiang, C., Cheng, J., Zheng, X., Wang, W., Chen, T., Ye, X., Li, J., & Feng, J. (2020). Transcript profiling provides insights into molecular processes during shoot elongation in temperature-sensitive peach (Prunus persica). Scientific Reports, 10(1). https://doi.org/10.1038/s41598-020-63952-2

26. Moodley, J. S., Krishna, S. B. N., Pillay, K., Sershen, N., & Govender, P. (2018). Green synthesis of silver nanoparticles from Moringa oleifera leaf extracts and its antimicrobial potential. Advances in Natural Sciences Nanoscience and Nanotechnology, 9(1), 015011. https://doi.org/10.1088/2043-6254/aaabb2

27. Nartop, P. (2022). Biomass and biochemical accumulations in ın vitro-grown Rubia tinctorum under the effect of different concentrations of biosynthetic silver nanoparticles. In Vitro Cellular & Developmental Biology - Plant, 58(5), 728–741. https://doi.org/10.1007/s11627-022-10287-4

28. Naseem, M., & Dandekar, T. (2012). The role of Auxin-Cytokinin antagonism in Plant-Pathogen interactions. PLoS Pathogens, 8(11), e1003026. https://doi.org/10.1371/journal.ppat.1003026

29. Nasiri, J., Rahimi, M., Hamezadeh, Z., Motamedi, E., & Naghavi, M. R. (2018). Fulfillment of green chemistry for synthesis of silver nanoparticles using root and leaf extracts of Ferula persica: Solid-state route vs. solution-phase method. Journal of Cleaner Production, 192, 514–530. https://doi.org/10.1016/j.jclepro.2018.04.218

30. Nazir, K., Hassan, S. W., Khan, M. I., Elamin, K. M. A., & Niyazi, H. A. (2023). The use of ZnO NPs and Ag NPs along with sterilizing agents for managing contamination in banana tissue culture. Biomass Conversion and Biorefinery, 14(23), 30297–30304. https://doi.org/10.1007/s13399-023-04623-w

31. Paladi, R. K., Rai, A. N., & Penna, S. (2017). Silver nitrate modulates organogenesis in Brassica juncea (L.) through differential antioxidant defense and hormonal gene expression. Scientia Horticulturae, 226, 261–267. https://doi.org/10.1016/j.scienta.2017.08.038

DOI: 10.31695/IJASRE.2025.10.1

32. Park, K., & Lee, Y. (2013). The stability of Citrate-Capped silver nanoparticles in isotonic glucose solution for intravenous injection. Journal of Toxicology and Environmental Health, 76(22), 1236–1245. https://doi.org/10.1080/15287394.2013.849215

33. Pokhrel, L. R., Dubey, B., & Scheuerman, P. R. (2013). Natural water chemistry (dissolved organic carbon, pH, and hardness) modulates colloidal stability, dissolution, and antimicrobial activity of citrate functionalized silver nanoparticles. Environmental Science Nano, 1(1), 45–54. https://doi.org/10.1039/c3en00017f

34. Pratiwi, D. E., Side, S., & Nisa, N. a. T. (2019). Synthesis of Silver Nanoparticles Using Moringa oleifera L. Leaf Extract as Bioreductor. Materials Science Forum, 967, 145–149. https://doi.org/10.4028/www.scientific.net/msf.967.145

35. Ospina, B., Lopez, V., Pantoja, A., Prakash, A., Gómez, H., & García, A. (2016). Cassava in the Caribbean region. In Instituto Interamericano De Cooperacion Para La Agricultura. Food and Agriculture Organization of the United Nations. https://repositorio.iica.int/bitstream/handle/11324/2665/BVE17038743i.pdf?sequence=1#:~:text=Cassava%20processing%20activities%20conducted%20manually%20and

36. Otekunrin, O. A. (2024). Cassava (*Manihot esculenta* Crantz): a global scientific footprint—production, trade, and bibliometric insights. Discover Agriculture, 2(1). https://doi.org/10.1007/s44279-024-00121-3

37. Pociecha, E., Gorczyca, A., Dziurka, M., Matras, E., & Oćwieja, M. (2021). Silver nanoparticles and silver ions differentially affect the phytohormone balance and yield in wheat. Agriculture, 11(8), 729. https://doi.org/10.3390/agriculture11080729

38. Quevedo, A., Ellis, L., Lynch, I., & Valsami-Jones, E. (2021). Mechanisms of silver nanoparticle uptake by embryonic zebrafish cells. Nanomaterials, 11(10), 2699. https://doi.org/10.3390/nano11102699

39. Ramasamy, M., Karuppiah, P., Ranganathan, H., Djearamane, S., Muthukrishnan, E., Kayarohanam, S., Arumugam, N., Almansour, A. I., & Wong, L. S. (2024). Nanomedicine potential of Cymbopogon citratus Linn. – Biogenic synthesized silver nanoparticles: A study on antimicrobial and anticancer efficacy. Journal of King Saud University - Science, 36(11), 103533. https://doi.org/10.1016/j.jksus.2024.103533

40. Rastogi, A., Zivcak, M., Tripathi, D., Yadav, S., & Kalaji, H. (2018). Phytotoxic effect of silver nanoparticles in Triticum aestivum: Improper regulation of photosystem I activity as the reason for oxidative damage in the chloroplast. Photosynthetica, 57(1), 209–216. https://doi.org/10.32615/ps.2019.019

41. Sarmast, M. K., & Salehi, H. (2021). Sub-lethal concentrations of silver nanoparticles mediate a phytostimulatory response in tobacco via the suppression of ethylene biosynthetic genes and the ethylene signaling pathway. In Vitro Cellular & Developmental Biology - Plant, 58(1), 1–14. https://doi.org/10.1007/s11627-021-10193-1

42. Shaikhaldein, H. O., Al-Qurainy, F., Nadeem, M., Khan, S., Tarroum, M., & Salih, A. M. (2020). Biosynthesis and characterization of silver nanoparticles using Ochradenus arabicus and their physiological effect on Maerua oblongifolia raised in vitro. Scientific Reports, 10(1). https://doi.org/10.1038/s41598-020-74675-9

43. Štefanić, P. P., Košpić, K., Lyons, D. M., Jurković, L., Balen, B., & Tkalec, M. (2021). Phytotoxicity of silver nanoparticles on tobacco plants: Evaluation of coating effects on photosynthetic performance and chloroplast ultrastructure. Nanomaterials, 11(3), 744. https://doi.org/10.3390/nano11030744

44. Sun, J., Wang, L., Li, S., Yin, L., Huang, J., & Chen, C. (2017). Toxicity of silver nanoparticles to Arabidopsis: Inhibition of root gravitropism by interfering with auxin pathway. Environmental Toxicology and Chemistry, 36(10), 2773–2780. https://doi.org/10.1002/etc.3833

DOI: 10.31695/IJASRE.2025.10.1

45. Syu, Y., Hung, J., Chen, J., & Chuang, H. (2014). Impacts of size and shape of silver nanoparticles on Arabidopsis plant growth and gene expression. Plant Physiology and Biochemistry, 83, 57–64. https://doi.org/10.1016/j.plaphy.2014.07.010

46. Tsuboi, A., Nakamura, K., & Kobayashi, N. (2013). A Localized Surface Plasmon Resonance-Based Multicolor Electrochromic Device with Electrochemically Size-Controlled Silver Nanoparticles. Advanced Materials, 25(23), 3197–3201. https://doi.org/10.1002/adma.201205214

47. Ugwoke, E., Aisida, S. O., Mirbahar, A. A., Arshad, M., Ahmad, I., Zhao, T., & Ezema, F. I. (2019). Concentration induced properties of silver nanoparticles and their antibacterial study. Surfaces and Interfaces, 18, 100419. https://doi.org/10.1016/j.surfin.2019.100419

48. Veselov, D., Langhans, M., Hartung, W., Aloni, R., Feussner, I., Götz, C., Veselova, S., Schlomski, S., Dickler, C., Bächmann, K., & Ullrich, C. I. (2003). Development of Agrobacterium tumefaciens C58-induced plant tumors and impact on host shoots are controlled by a cascade of jasmonic acid, auxin, cytokinin, ethylene and abscisic acid. Planta, 216(3), 512–522. https://doi.org/10.1007/s00425-002-0883-5

49. Wang, L., Sun, J., Lin, L., Fu, Y., Alenius, H., Lindsey, K., & Chen, C. (2019). Silver nanoparticles regulate Arabidopsis root growth by concentration-dependent modification of reactive oxygen species accumulation and cell division. Ecotoxicology and Environmental Safety, 190, 110072. https://doi.org/10.1016/j.ecoenv.2019.110072

50. Yanık, F., & Vardar, F. (2019). Assessment of silver nanoparticle-induced morphological, biochemical and physiological alterations in wheat roots. Annali Di Botanica, 9, 83–94. https://doi.org/10.13133/2239-3129/14633

51. Zhao, Y., & Hasenstein, K. H. (2009). Primary root growth regulation: the role of Auxin and Ethylene antagonists. Journal of Plant Growth Regulation, 28(4), 309–320. https://doi.org/10.1007/s00344-009-9095-6

*Corresponding author: ddaniels@ub.edu.bz

DOI: 10.31695/IJASRE.2025.10.1